EUROPEAN ORGANIZATION FOR NUCLEAR RESEARCH

Systematic studies of correlations between different order flow harmonics in Pb–Pb collisions at $\sqrt{s_{\mathrm{NN}}} = 2.76$ TeV

ALICE Collaboration*

Abstract

The correlations between event-by-event fluctuations of anisotropic flow harmonic amplitudes have been measured in Pb–Pb collisions at $\sqrt{s_{\mathrm{NN}}} = 2.76$ TeV with the ALICE detector at the Large Hadron Collider. The results were obtained with the multi-particle correlation observables dubbed symmetric cumulants. These observables are robust against biases originating from non-flow effects. The centrality dependence of correlations between the higher order harmonics (v_3, v_4 and v_5) and the lower order harmonics (v_2 and v_3), as well as the transverse momentum dependence of correlations between v_3 and v_2 and between v_4 and v_2 are presented. The results are compared to calculations from viscous hydrodynamics and A Multi-Phase Transport (AMPT) model calculations. The comparisons to viscous hydrodynamic models demonstrate that the different order harmonic correlations respond differently to the initial conditions and the temperature dependence of the ratio of shear viscosity to entropy density (η/s). A small η/s is favored regardless of initial conditions and the AMPT initial condition yields results closest to the measurements. Correlations between the magnitudes of v_2, v_3 and v_4 magnitudes show moderate p_{T} dependence in mid-central collisions. This might be an indication of possible viscous corrections to the equilibrium distribution at hadronic freeze-out, which might help to understand the possible contribution of bulk viscosity in the hadronic phase of the system. Together with existing measurements of individual flow harmonics, the results presented here provide further constraints on initial conditions and the transport properties of the system produced in heavy-ion collisions.

---

*See Appendix A for the list of collaboration members

1 Introduction

The main emphasis of the ultra-relativistic heavy-ion collision programs at the Relativistic Heavy Ion Collider (RHIC) and the Large Hadron Collider (LHC) is to study the deconfined phase of strongly interacting nuclear matter, the Quark-Gluon Plasma (QGP). This matter exhibits strong collective and anisotropic flow in the plane transverse to the beam direction, which is driven by anisotropic pressure gradients, resulting in more particles emitted in the direction of the largest gradients. The large elliptic flow discovered at RHIC energies [1] is also observed at LHC energies [2, 3]. This has been predicted by calculations utilizing viscous hydrodynamics [4–9]. These calculations also demonstrated that the shear viscosity to the entropy density ratio (η/s) of the QGP in heavy-ion collisions at RHIC and LHC energies is close to a universal lower bound $1/4\pi$ [10].

The temperature dependence of η/s has some generic features that most known fluids obey. For instance, one such general behavior is that the ratio typically reaches its minimum value close to the phase transition region [11]. It was shown, using kinetic theory and quantum mechanical considerations [12], that $\eta/s \sim 0.1$ would be the correct order of magnitude for the lowest possible shear viscosity to entropy density ratio value found in nature. Later it was demonstrated that an exact lower bound $(\eta/s)_{\mathrm{min}} = 1/4\pi \approx 0.08$ can be calculated using AdS/CFT correspondence [10]. Hydrodynamical simulations also support the view that η/s of the QGP is close to that limit [8]. This may have important implications for other fundamental physics goals. It is argued that such a low value might imply that thermodynamic trajectories for the expanding matter would lie close to the quantum chromodynamics (QCD) critical end point, which is another subject of intensive experimental study [11, 13].

Anisotropic flow [14] is traditionally quantified with n^{th}-order flow coefficients v_n and corresponding symmetry plane angles Ψ_n in a Fourier decomposition of the particle azimuthal distribution in the plane transverse to the beam direction [15]:

$$E\frac{\mathrm{d}^3N}{\mathrm{d}p^3} = \frac{1}{2\pi}\frac{\mathrm{d}^2N}{p_{\mathrm{T}}\mathrm{d}p_{\mathrm{T}}\mathrm{d}\eta}\left\{1 + 2\sum_{n=1}^{\infty} v_n(p_{\mathrm{T}},\eta)\cos[n(\varphi - \Psi_n)]\right\}, \tag{1}$$

where E, p, p_{T}, φ and η are the particle's energy, momentum, transverse momentum, azimuthal angle and pseudorapidity, respectively, and Ψ_n is the azimuthal angle of the symmetry plane of the nth-order harmonic. v_n can be calculated as $v_n = \langle\cos[n(\varphi - \Psi_n)]\rangle$, where the brackets denote an average over all particles in all events. The anisotropic flow in heavy-ion collisions is typically understood as the hydrodynamic response of the produced matter to spatial deformations of the initial energy density profile [16]. This profile fluctuates event-by-event due to fluctuating position of the constituents inside the colliding nuclei, which implies that v_n also fluctuates [17, 18]. The recognition of the importance of flow fluctuations led to the discovery of triangular and higher flow harmonics [19, 20] as well as to the correlation between different v_n harmonics [21, 22]. The higher order harmonics are expected to be sensitive to fluctuations in the initial conditions and to the magnitude of η/s [23, 24], while v_n correlations have the potential to discriminate between these two respective contributions [21].

Difficulties in extracting η/s in heavy-ion collisions can be attributed mostly to the fact that it strongly depends on the specific choice of the initial conditions in the models used for comparison [4, 24, 25]. Viscous effects also reduce the magnitude of the elliptic flow. Furthermore, the magnitude of η/s used in hydrodynamic calculations should be considered as an average over the temperature evolution of the expanding fireball as it is known that η/s depends on temperature. In addition, part of the elliptic flow can also originate from the hadronic phase [26–28]. Therefore, both the temperature dependence of η/s and the relative contributions from the partonic and hadronic phases should be understood better to quantify the η/s of the QGP.

An important input to the hydrodynamic model simulations is the initial distribution of energy density

in the transverse plane (the initial density profile), which is usually estimated from the probability distribution of nucleons in the incoming nuclei. This initial energy density profile can be quantified by calculating the distribution of the spatial eccentricity [19],

$$\varepsilon_n e^{in\Phi_n} = -\{r^n e^{in\phi}\}/\{r^n\}, \tag{2}$$

where the curly brackets denote the average over the transverse plane, i.e., $\{\cdots\} = \int dxdy \; e(x,y,\tau_0)$ $(\cdots)$, r is the distance to the system's center of mass, $e(x,y,\tau_0)$ is the energy density at the initial time τ_0, and Φ_n is the participant plane angle (see Ref. [29, 30]). There is experimental and theoretical evidence [19, 20, 31] that the harmonic coefficients, v_2 and v_3, are to a good approximation linearly proportional to the deformations in the initial energy density in the transverse plane (e.g. $v_n \propto \varepsilon_n$ for n=2 or 3). v_4 and higher order flow coefficients can arise from initial anisotropies in the same harmonic [19, 29, 32, 33] (linear response) or can be induced by lower-order harmonics [34, 35] (nonlinear response). The higher harmonics ($n > 3$) can be understood as superpositions of linear and nonlinear responses, through which they are correlated with lower order harmonics [32, 33, 35, 36]. When the order of the harmonic is large, the nonlinear response contribution in viscous hydrodynamics is dominant and increases in more peripheral collisions [35, 36]. The magnitude of the viscous corrections as a function of p_T for v_4 and v_5 is sensitive to the ansatz used for the viscous distribution function, a correction for the equilibrium distribution at hadronic freeze-out [36, 37]. Hence, studies of the higher order ($n > 3$) to lower order (v_2 or v_3) harmonic correlations and their p_T dependence can help to understand the viscous correction to the momentum distribution at hadronic freeze-out which is among the least understood parts of hydrodynamic calculations [30, 36, 38, 39].

Recently, the ALICE Collaboration measured for the first time the Symmetric 2-harmonic 4-particle Cumulants (SC), new multiparticle observables which quantify the relationship between event-by-event fluctuations of two different flow harmonics [40]. The new observables are particularly robust against few-particle non-flow correlations and they provide independent information to recently analyzed symmetry plane correlators. It was demonstrated that they are sensitive to the temperature dependence of η/s of the expanding medium and therefore simultaneous descriptions of correlations between different order harmonics would constrain both the initial conditions and the medium properties [40, 41]. In this article, we have extended the analysis of SC observables to higher order Fourier harmonics (up to 5th order) as well as measured the p_T dependence of correlations for the lower order harmonics (v_3-v_2 and v_4-v_2). We also include extensive comparisons to hydrodynamic and AMPT model calculations. In Sec. 2 we summarize our findings from the previous work [40] and present the analysis methods. The experimental setup and measurements are described in Sec. 3 and the sources of systematic uncertainties are explained in Sec. 4. The results of the measurements are presented in Sec. 5. In Sec. 6 we present comparisons to theoretical calculations. Various theoretical models used in this article are described in Sec. 6. Sec. 7 summarizes our findings.

2 Experimental Observables

Existing measurements provide an estimate of the average value of η/s of the QGP, both at RHIC and LHC energies. What remains uncertain is how the η/s of the QGP depends on temperature (T). The temperature dependence of η/s in the QGP was discussed in [13]. The effects on hadron spectra and elliptic flow were studied in [42] for different parameterizations of $\eta/s(T)$. A more systematic study with event-by-event EKRT+viscous hydrodynamic calculations has just been initiated in Ref. [30], where the first (and only rather qualitative) possibilities were investigated (see Fig. 1 therein). The emerging picture is that the study of individual flow harmonics v_n alone are unlikely to reveal the details of the temperature dependence of η/s. It was already demonstrated in [30] that different $\eta/s(T)$ parameterizations can lead to the same centrality dependence of individual flow harmonics. In Ref. [21] new flow observables were introduced which quantify the degree of correlation between two different harmonics v_m and v_n.

113 These new observables have the potential to discriminate between the contributions to anisotropic flow
114 development from initial conditions and from the transport properties of the QGP [21]. Therefore their
115 measurement would provide experimental constraints on theoretical predictions for the individual stages
116 of heavy-ion system evolution independently. In addition, it turned out that correlations of different flow
117 harmonics are sensitive to the temperature dependence of η/s [40], to which individual flow harmonics
118 are weakly sensitive [30].

119 For reasons discussed in [40, 43], the correlations between different flow harmonics cannot be studied
120 experimentally with the same set of observables introduced in [21]. Based on [43], new flow observables
121 obtained from multiparticle correlations, *Symmetric Cumulants (SC)*, were introduced. SC observables
122 are nearly insensitive to nonflow and quantify the correlation of the amplitudes of two different flow har-
123 monics. The first measurements of SC observables were recently published by the ALICE Collaboration
124 in [40].

125 The SC observables are defined as:

$$
\begin{aligned}
\langle\langle\cos(m\varphi_1+n\varphi_2-m\varphi_3-n\varphi_4)\rangle\rangle_c &= \langle\langle\cos(m\varphi_1+n\varphi_2-m\varphi_3-n\varphi_4)\rangle\rangle \\
&\quad - \langle\langle\cos[m(\varphi_1-\varphi_2)]\rangle\rangle \langle\langle\cos[n(\varphi_1-\varphi_2)]\rangle\rangle \\
&= \langle v_m^2 v_n^2\rangle - \langle v_m^2\rangle\langle v_n^2\rangle,
\end{aligned} \tag{3}
$$

126 with the condition $m \neq n$ for two positive integers m and n (for details see Sec. IV C in [43]). In this
127 article SC(m,n) normalized by the product $\langle v_m^2\rangle\langle v_n^2\rangle$ [40, 44] is denoted by NSC(m,n):

$$
\text{NSC}(m,n) \equiv \frac{\text{SC}(m,n)}{\langle v_m^2\rangle\langle v_n^2\rangle}. \tag{4}
$$

128 Normalized symmetric cumulants reflect only the strength of the correlation which is expected to be
129 insensitive to the magnitudes of v_m and v_n, while SC(m,n) has contributions from both the correlations
130 between the two different flow harmonics and the individual v_n harmonics. In Eq. (4) the products in the
131 denominator are obtained from two-particle correlations using a pseudorapidity gap of $|\Delta\eta| > 1.0$ which
132 suppresses biases from few-particle nonflow correlations. For the two two-particle correlations which
133 appear in the definition of SC(m,n) in Eq. (3) the pseudorapidity gap is not needed, since nonflow is
134 suppressed by construction in this case. This was verified by HIJING model simulations in [40].

135 The ALICE measurements [40] have revealed that fluctuations of v_2 and v_3 are anti-correlated, while
136 fluctuations of v_2 and v_4 are correlated in all centralities [40]. However, the details of the centrality de-
137 pendence differ in the fluctuation-dominated (most central) and the geometry-dominated (mid-central)
138 regimes [40]. The observed centrality dependence of SC(4,2) cannot be captured by models with constant
139 η/s, indicating clearly that the temperature dependence of η/s plays an important role. These results
140 were also used to discriminate between different parameterizations of initial conditions. It was demon-
141 strated that in the fluctuation-dominated regime (central collisions), MC-Glauber initial conditions with
142 binary collision weights are favored over wounded nucleon weights [40].

3 Data Analysis

144 Data recorded by ALICE in Pb–Pb collisions at $\sqrt{s_{\text{NN}}} = 2.76$ TeV during the 2010 heavy-ion run at the
145 LHC is used for this analysis. Detailed descriptions of the ALICE detector can be found in [45–47].
146 The Time Projection Chamber (TPC) was used to reconstruct charged particle tracks and measure their
147 momenta with full azimuthal coverage in the pseudorapidity range $|\eta| < 0.8$. Two scintillator arrays (V0)
148 which cover the pseudo-rapidity ranges $-3.7 < \eta < -1.7$ and $2.8 < \eta < 5.1$ were used for triggering and
149 the determination of centrality [48]. The trigger conditions and the event selection criteria are identical to
150 those described in [2, 48]. Approximately 10^7 minimum-bias Pb–Pb events with a reconstructed primary

151 vertex within ± 10 cm from the nominal interaction point along the beam direction are selected. Charged
152 particles reconstructed in the TPC in $|\eta| < 0.8$ and $0.2 < p_T < 5$ GeV/c were selected. The charged track
153 quality cuts described in [2] were applied to minimize contamination from secondary charged particles
154 and fake tracks. The track reconstruction efficiency and contamination were estimated from HIJING
155 Monte Carlo simulations [49] combined with a GEANT3 [50] detector model and were found to be
156 independent of the collision centrality. The reconstruction efficiency increases from 70% to 80% for
157 particles with $0.2 < p_T < 1$ GeV/c and remains constant at $(80 \pm 5)\%$ for $p_T > 1$ GeV/c. The estimated
158 contamination by secondary charged particles from weak decays and photon conversions is less than 6%
159 at $p_T = 0.2$ GeV/c and falls below 1% for $p_T > 1$ GeV/c. The p_T cut-off of 0.2 GeV/c reduces event-
160 by-event biases due to small reconstruction efficiency at lower p_T, while the high p_T cut-off of 5 GeV/c
161 reduces the effect of jets on the measured correlations. Reconstructed TPC tracks were required to have
162 at least 70 space points (out of a maximum of 159). Only tracks with a transverse distance of closest
163 approach (DCA) to the primary vertex less than 3 mm, both in the longitudinal and transverse directions,
164 are accepted. This reduces the contamination from secondary tracks produced in the detector material,
165 particles from weak decays, etc. Tracks with kinks (i.e, tracks that appear to change direction due to
166 multiple scattering or $K^{\pm}$ decays) were rejected.

4   Systematic Uncertainties

168 The systematic uncertainties are estimated by varying the event and track selection criteria. All system-
169 atic checks described here are performed independently. The SC(m,n) values resulting from each vari-
170 ation are compared to ones from the default event and track selection described in the previous section,
171 and differences are taken as the systematic uncertainty due to each individual source. The contributions
172 from different sources were added in quadrature to obtain the total systematic uncertainty.

173 The event centrality was determined by the V0 detectors [51] with better than 2% resolution. The sys-
174 tematic uncertainty from the centrality determination was evaluated by using the TPC and Silicon Pixel
175 Detector (SPD) [52] detectors instead of the V0 detectors. The systematic uncertainty from the centrality
176 determination is about 3% both for SC(5,2) and SC(4,3), and 8% for SC(5,3).

177 As described in Sec. 3, the reconstructed vertex position along the beam axis (z-vertex) is required to be
178 located within 10 cm of the interaction point (IP) to ensure uniform detector acceptance for tracks within
179 $|\eta| < 0.8$. The systematic uncertainty from the z-vertex cut was estimated by reducing the z-vertex range
180 to 8cm and was found to be less than 3%.

181 The analyzed events were recorded with two settings of the magnet polarity and the resulting data sets
182 have almost equal numbers of events. Events with both magnet polarities were used in the default analy-
183 sis, and the systematic uncertainties were evaluated from the variation between each of the two magnetic
184 field settings. The uncertainty on the p_T dependent track reconstruction efficiency was also taken into
185 account. Magnetic polarity variation and reconstruction efficiency effects contribute less than 2% to the
186 systematic uncertainty.

187 The systematic uncertainty due to the track reconstruction was estimated from comparisons between
188 results for the so-called standalone TPC tracks with the same parameters as described in Sec. 3, and tracks
189 from a combination of the TPC and the Inner Tracking System (ITS) detectors with tighter selection
190 criteria. To correct for non-uniform azimuthal acceptance due to dead zones in the SPD, and to get the
191 best transverse momentum resolution, approach of hybrid selection with SPD hit and/or ITS refit tracks
192 combined with TPC were used. Then each track reconstruction strategy was evaluated by varying the
193 threshold on parameters used to select the tracks at the reconstruction level. The systematic difference
194 of up to 12% was observed in SC(m,n) from the different track selections. In addition, we applied
195 the like-sign technique to estimate non-flow contributions to SC(m,n). The difference between results
196 obtained by selecting all charged particles and results obtained after either selecting only positively or

5

197 only negatively charged particles was the largest contribution to the systematic uncertainty and it is about
198 7% for SC(4,3) and 20% for SC(5,3).

199 Another large contribution to the systematic uncertainty originates from azimuthal non-uniformities in
200 the efficiency. In order to estimate its effects, we use the AMPT model (see Sec. 6) which has a uniform
201 distribution in azimuthal angle. Detector inefficiencies were introduced to mimic the non-uniform az-
202 imuthal distribution in the data. For the observables SC(5,2), SC(5,3) and SC(4,3) the variation due to
203 non-uniform acceptance is about 9%, 17% and 11%, respectively. Overall, the systematic uncertainties
204 are larger for SC(5,3) and SC(5,2) than for the lower harmonics of SC(m,n). This is because v_n decreases
205 with increasing n and becomes more sensitive to azimuthal modulation due to detector imperfections.

5 Results

207 The centrality dependence of the higher order harmonic correlations (SC(4,3), SC(5,2) and SC(5,3)) are
208 presented in Fig. 1 and compared to the lower order harmonic correlations (SC(4,2) and SC(3,2)) which
209 were measured in [40]. The correlation between v_3 and v_4 is negative, and similarly for v_3 and v_2, while
210 the other correlations are all positive, which reveals that v_2 and v_5 as well as v_3 and v_5 are correlated like
211 v_2 and v_4, while v_3 and v_4 are anti-correlated like v_3 and v_2.
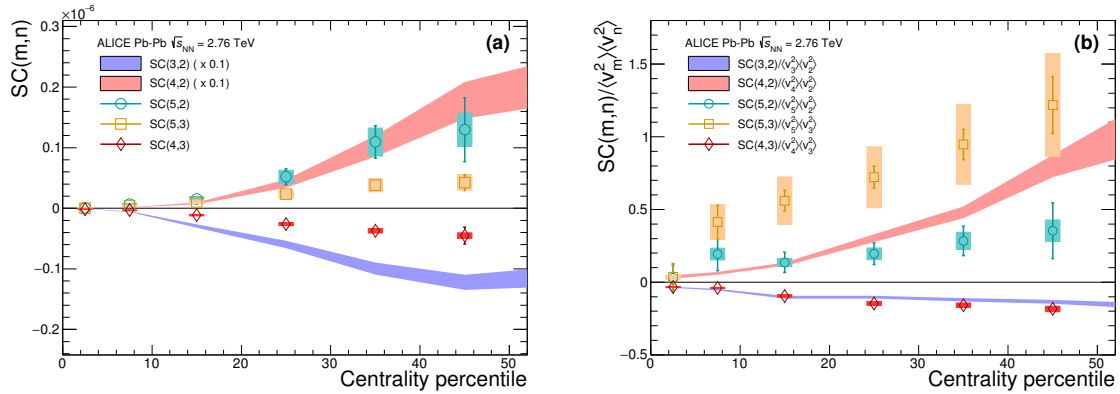

Fig. 1: SC(m,n) (a) and NSC(m,n) (b) with flow harmonic up to 5th order in Pb–Pb collisions at $\sqrt{s_{NN}} = 2.76$ TeV. The lower order harmonic correlations (SC(3,2), SC(4,2), NSC(3,2) and NSC(4,2)) are taken from [40] and shown as bands. Note that the systematic and statistical errors are combined in quadrature for these lower order harmonic correlations and SC(4,2) and SC(3,2) are scaled by a factor of 0.1. Systematical errors are represented with boxes.

212 The higher order flow harmonic correlations (SC(4,3), SC(5,2) and SC(5,3)) are much smaller compared
213 to the lower order harmonic correlations. In particular SC(5,2) is 10 times smaller than SC(4,2) and
214 SC(4,3) is about 20 times smaller that SC(3,2).

215 However, unlike SC(m,n), the NSC(m,n) results with the higher order flow harmonics show almost
216 the same order of the correlation strength as the lower order flow harmonic correlations (NSC(3,2) or
217 NSC(4,2)). The NSC(4,3) magnitude is comparable to NSC(3,2) and one finds that a hierarchy, NSC(5,3)
218 > NSC(4,2) > NSC(5,2), holds for centrality ranges > 20% within the errors as shown in Fig. 1b.
219 These results indicate that the lower order harmonic correlations are larger than higher order harmonic
220 correlations, not only because of the correlation strength itself but also because of the strength of the
221 individual flow harmonics. SC(5,2) is stronger than SC(5,3), but the normalized correlation between v_5
222 and v_3 is stronger than the normalized correlation between v_5 and v_2.

223 It can be seen in Fig. 1a that the lower order harmonic correlations (SC(3,2) and SC(4,2)) as well as
224 SC(5,2) increase non-linearly towards peripheral collisions. In the case of SC(5,3) and SC(4,3), the
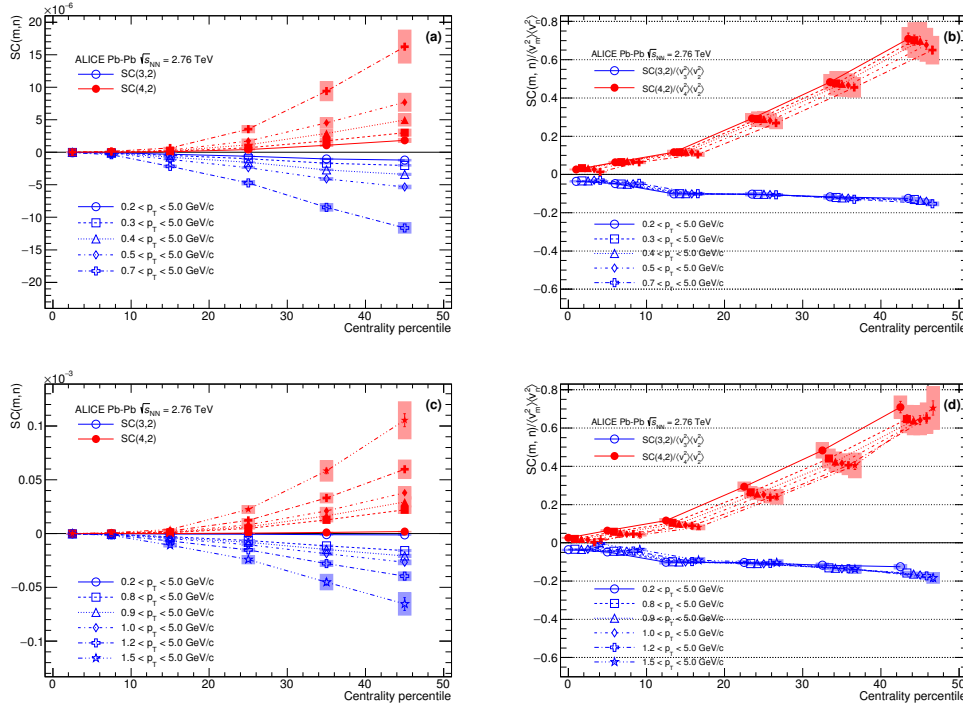
Fig. 2: SC(3,2) and SC(4,2) with low (a) and high (c) minimum p_T cuts, and normalized SC(3,2) and SC(4,2) ((b) and (d)) in Pb–Pb collisions at $\sqrt{s_{NN}} = 2.76$ TeV. Panels (a) and (b) show the results for the minimum p_T range $0.2 < p_T < 0.7$ GeV/c and panels (c) and (d) are for the minimum p_T range $0.8 < p_T < 1.5$ GeV/c. Note that NSC data points from each minimum p_T in a centrality percentile bin are shifted for visibility.

centrality dependence is weaker than for the other harmonic correlations and a monotonic increase is observed. NSC(5,3) shows the strongest correlation among all harmonics while NSC(5,2) shows a weak centrality dependence. Both NSC(3,2) and NSC(4,3) show a monotonic increase toward peripheral collisions with the similar magnitude.

To study the p_T dependence of SC(m,n), we systematically vary the low p_T cut-off, instead of using independent p_T intervals, in order to avoid large statistical fluctuations in the results. Various minimum p_T cuts from 0.2 to 1.5 GeV/c are applied. The p_T-dependent results for SC(3,2) and SC(4,2) with minimum p_T cuts $0.2 < p_T < 0.7$ GeV/c are shown in Fig. 2a. The strength of SC(m,n) becomes larger as the minimum p_T increases. These p_T dependent correlations have much stronger centrality dependence, with SC(m,n) getting much larger as the centrality or the minimum p_T cut increase. NSC(3,2) and NSC(4,2) with different minimum cuts are shown in Figs. 2b and 2d. The strong p_T dependence observed in SC(m,n) is not seen in NSC(m,n). The NSC(m,n) results are consistent within the errors for all minimum p_T cuts. This indicates that the p_T dependence of SC(m,n) is dominated by the p_T dependence of the $\langle v_n \rangle$ values. The minimum p_T cuts are extended from 0.8 to 1.5 GeV/c and the results are shown in Fig. 2c and 2d. While SC(m,n) shows similar trends as for $p_T < 0.8$ GeV/c, NSC(m,n) tends to decrease with increasing p_T. The p_T-dependence of NSC(3,2) is not clearly seen and it is consistent with no p_T dependence within the statistical and systematic errors for the centrality range <30%, while showing a moderate decreasing trend with increasing p_T for the >30% centrality range. NSC(4,2) shows a moderate decreasing trend as p_T increases. These observations are strikingly different from p_T dependence of the individual flow harmonics, where the relative flow fluctuations $\sigma_{v_2}/\langle v_2 \rangle$ [53] are independent of momentum up to $p_T \sim 8$ GeV/c (see Fig. 3 in Ref. [54]).

6 Model Comparisons

We have compared the centrality dependence of our observables with event-by-event EKRT+viscous hydrodynamic calculations [30], where the initial energy density profiles are calculated using a next-to-leading order perturbative-QCD+saturation model [55, 56]. The subsequent spacetime evolution is described by relativistic dissipative fluid dynamics with different parameterizations for the temperature dependence of the shear viscosity to entropy density ratio $\eta/s(T)$. This model gives a good description of the charged hadron multiplicity and the low p_T region of the charged hadron spectra at RHIC and the LHC (see Figs. 11-13 in [30]). Each of the $\eta/s(T)$ parameterizations is adjusted to reproduce the measured v_n from central to mid-peripheral collisions (see Fig. 14 in [30]).

The VISH2+1 [57, 58] event-by-event calculations for relativistic heavy-ion collisions are based on (2+1)-dimensional viscous hydrodynamics which describes both the QGP phase and the highly dissipative and even off-equilibrium late hadronic stage with fluid dynamics. With well-tuned transport coefficients and decoupling temperature, and given initial condition discussed later, it can describe the p_T spectra and different flow harmonics at RHIC and the LHC [5, 57, 59, 60]. Three different initial conditions (MC-Glauber, MC-KLN and AMPT) along with different constant η/s values are used in the model [41]. Traditionally, the Glauber model constructs the initial entropy density with contributions from the wounded nucleon and binary collision density profiles [61], and the KLN model assumes that the initial entropy density is proportional to the initial gluon density calculated from the corresponding k_T factorization formula [62]. In the Monte Carlo versions (MC-Glauber and MC-KLN) [63–65], additional initial state fluctuations are introduced through position fluctuations of individual nucleons inside the colliding nuclei. For the AMPT initial conditions [60, 66, 67], the fluctuating energy density profiles are constructed from the energy decompositions of individual partons, which fluctuate in both momentum and position coordinate. Compared with the MC-Glauber and MC-KLN initial conditions, the additional Gaussian smearing in the AMPT initial conditions gives rise to non-vanishing initial local flow velocities [66].

The centrality dependence of the SC observables is compared to that in the AMPT model [68–70]. Even though thermalization could be achieved in collisions of very large nuclei and/or at extremely high energy [71], the dense matter created in heavy-ion collisions may not reach full thermal or chemical equilibrium as a result of its finite volume and short lifetime. To address such non-equilibrium many-body dynamics, AMPT has been developed, which includes both initial partonic and final hadronic interactions and the transition between these two phases of matter. For the initial conditions, the AMPT model uses the spatial and momentum distributions of hard minijet partons and soft strings from the HIJING model [49, 72]. The AMPT model can be run in two main configurations, the default and the string melting model [1]. In the default version, partons are recombined with their parent strings when they stop interacting. The resulting strings are later converted into hadrons using the Lund string fragmentation model [73, 74]. In the string melting version, the initial strings are melted into partons whose interactions are described by the ZPC parton cascade model [75]. These partons are then combined into the final state hadrons via a quark coalescence model. In both configurations, the dynamics of the subsequent hadronic matter is described by a hadronic cascade based on A Relativistic Transport (ART) model [76] which also includes resonance decays. The third version used in this article is based on the string melting configuration in which the hadronic rescattering phase is switched off to study its influence on the development of anisotropic flow. Even though the string melting version of AMPT [70, 77] reasonably reproduces particle yields, p_T spectra, and v_2 of low-p_T pions and kaons in central and mid-central Au–Au collisions at $\sqrt{s_{NN}} = 200$ GeV and Pb–Pb collisions at $\sqrt{s_{NN}} = 2.76$ TeV [78], it was seen clearly in a recent study [79] that it fails to quantitatively reproduce the harmonic flow coefficients of identified hadrons (v_2, v_3, v_4 and v_5) at $\sqrt{s_{NN}} = 2.76$ TeV. It turns out that the radial flow in AMPT is 25% lower than that

---

[1]The input parameters used in both configurations are: $\alpha_s = 0.33$, a partonic cross-section of 1.5 mb, while the Lund string fragmentation parameters were set to $\alpha = 0.5$ and $b = 0.9$ GeV^{-2}.

292   measured at the LHC, which is responsible for the quantitative disagreement [79]. The details of the
293   AMPT configurations used in this article and the comparisons of p_T-differential v_n for pions, kaons and
294   protons to the data can be found in [79].

6.1   Low Order Harmonic Correlations

296   SC(3,2) and SC(4,2) are compared to several theoretical calculations. The event-by-event EKRT+viscous
297   hydrodynamic predictions with the different parameterizations for the temperature dependence of the
298   shear viscosity to entropy density ratio $\eta/s(T)$ are shown in Fig. 2 of Ref. [40]. In this previous work it
299   was demonstrated that NSC(3,2) is sensitive mainly to the initial conditions, while NSC(4,2) is sensitive
300   to both the initial conditions and the system properties, which is consistent with the predictions from [21].
301   However, the sign of NSC(3,2) is negative in the data in 0-10% central collisions while it is positive in
302   the models where the anisotropies originate mainly from fluctuations. This observation helps us to better
303   understand the fluctuations in initial energy density. NSC(4,2) observable shows better sensitivity for
304   different $\eta/s(T)$ parameterizations but the model cannot describe either the centrality dependence or
305   the absolute values. This observed discrepancy between data and theoretical predictions indicates that
306   the current understanding of initial conditions used to model the initial stages of heavy-ion collisions
307   needs to be revisited to further constrain $\eta/s(T)$. The use of SC(m,n) and NSC(m,n) can provide new
308   constraints for the detailed modeling of fluctuating initial conditions. The better constraints on the initial
309   state conditions will certainly reduce the uncertainties in determining $\eta/s(T)$.

310   The comparison to the VISH2+1 calculation [41] is shown in Fig. 3. All calculations with large η/s
311   regardless of the initial conditions ($\eta/s = 0.2$ for MC-KLN and MC-Glauber initial conditions and
312   $\eta/s = 0.16$ for AMPT initial conditions) fail to capture the centrality dependence of SC(3,2) and SC(4,2).
313   Among the calculations with small η/s ($\eta/s = 0.08$), the one with the AMPT initial condition describes
314   the data better both for SC(3,2) and SC(4,2) but it cannot describe the data quantitively for most of
315   the centrality ranges. Similar to the event-by-event EKRT+viscous hydrodynamic calculations [30], the
316   sign of the normalized NSC(3,2) in the model calculations in Fig 3 is opposite to that in data in 0-10%
317   central collisions. NSC(3,2) does not show sensitivity to the initial conditions nor to the different η/s
318   parameterizations used in the models and cannot be described quantitatively by these models. However,
319   NSC(4,2) is sensitive both to the initial conditions and the η/s parameterizations used in the models.
320   Even though NSC(4,2) favors both AMPT initial conditions with $\eta/s = 0.08$ and MC-Glauber initial
321   conditions with $\eta/s = 0.20$, SC(4,2) can only be described by models with smaller η/s. Hence the
322   calculation with large $\eta/s = 0.20$ is ruled out. We conclude that η/s should be small and that AMPT
323   initial conditions are favored by the data.

324   SC(m,n) calculated from AMPT simulations are compared with data in Fig. 4. For SC(3,2), the calcu-
325   lation with the default AMPT settings is closet to the data, but none of the AMPT configurations can
326   describe the data fully. The same default calculation can describe the sign and magnitude of NSC(3,2)
327   while the hydrodynamic calculations fail to describe either of them in the most central collisions. Inter-
328   estingly, the string melting AMPT configuration cannot reproduce the data, and the resulting correlations
329   are weaker than in data. The third version based on the string melting configuration without the hadronic
330   rescattering phase is also shown. The hadronic rescattering stage makes both SC(3,2) and NSC(3,2)
331   stronger in the string melting AMPT model but not enough to describe the data. Further investigations
332   proved why the default AMPT model can describe NSC(3,2) fairly well but underestimates SC(3,2).
333   By taking the differences in the individual flow harmonics (v_2 and v_3) between the model and data into
334   account, it was possible to recover the difference in SC(3,2) between the data and the model. The dis-
335   crepancy in SC(3,2) can be explained by the overestimated individual v_n values as reported in [79] in all
336   the centrality ranges.

337   In the case of SC(4,2), the string melting AMPT model can describe the data fairly well while the de-
338   fault model underestimates it. NSC(4,2) is slightly overestimated by the string melting setting which
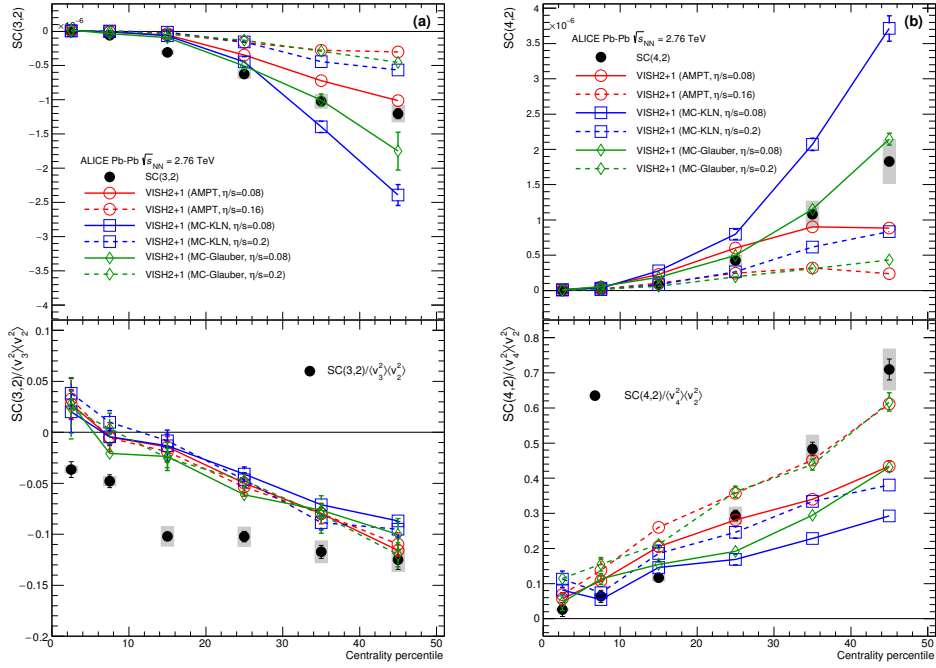
Fig. 3: SC(3,2) (a) and SC(4,2) (b) in Pb–Pb collisions at $\sqrt{s_{\mathrm{NN}}} = 2.76$ TeV are compared to various VISH2+1 calculations [41] with different settings. Upper (lower) panels show SC(m,n) (NSC(m,n)). Calculations with AMPT, MC-KLN, and MC-Glauber initial conditions are drawn as different colors and markers. The η/s parameters are shown in line styles, the small $\eta/s = 0.08$ are shown as solid lines, and large η/s (0.2 for MC-KLN and MC-Glauber, 0.16 for AMPT) are drawn as dashed lines.
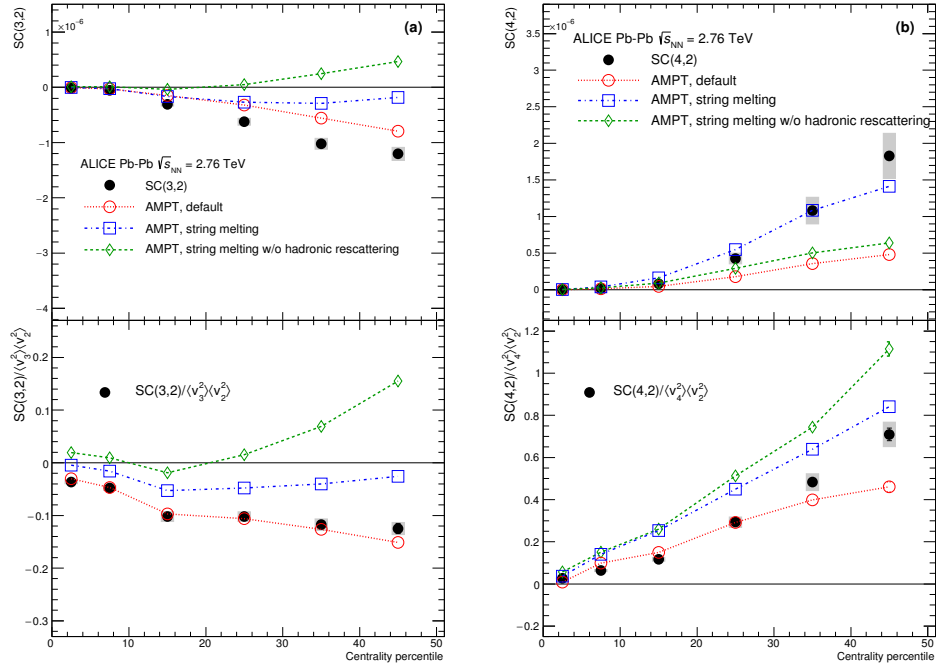
Fig. 4: SC(3,2) (a) and SC(4,2) (b) in Pb–Pb collisions at $\sqrt{s_{\mathrm{NN}}} = 2.76$ TeV are compared to various AMPT models. Upper (lower) panels show SC(m,n) (NSC(m,n)).

10
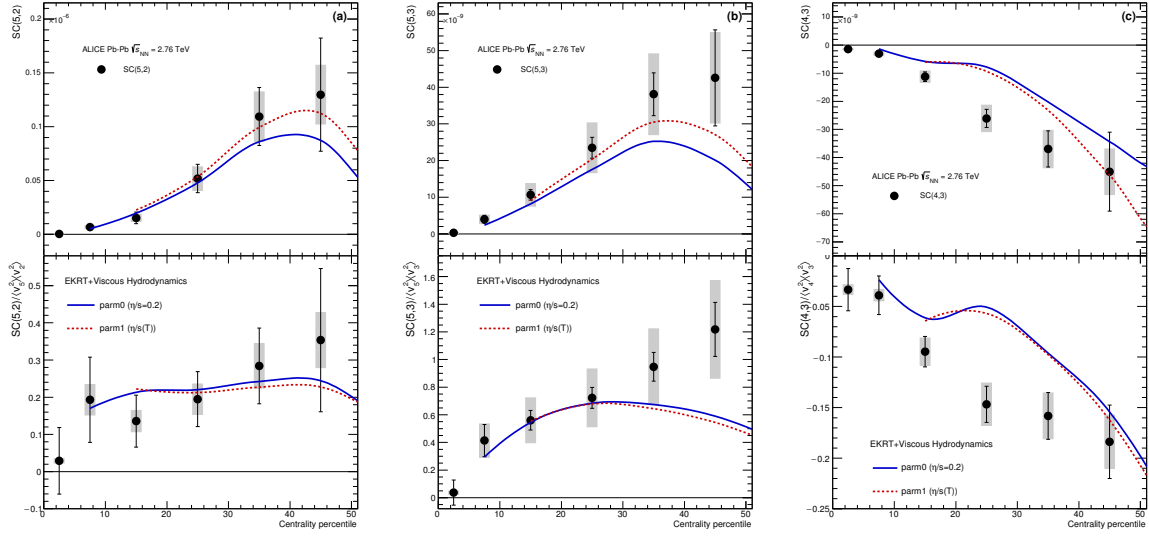
Fig. 5: Measurements of SC(5,2) (a), SC(5,3) (b) and SC(4,3) (c) in Pb–Pb collisions at $\sqrt{s_{\mathrm{NN}}} = 2.76$ TeV are compared to the event-by-event EKRT+viscous hydrodynamic calculations [30]. The lines are hydrodynamic predictions with two different $\eta/s(T)$ parameterizations, labeled in the same way as in [30]. Upper (lower) panels show SC(m,n) (NSC(m,n)).

can describe SC(4,2) but the default AMPT configuration can describe the data better. The influence of the hadronic rescattering phase on NSC(4,2) is opposite to other observables (SC(3,2), NSC(3,2) and SC(4,2)). The hadronic rescattering makes NSC(4,2) slightly smaller. It should be noted that the agreement with SC(m,n) should not be overemphasized since there are discrepancies in the individual v_n between the AMPT models and the data as was demonstrated for SC(3,2). Hence the simultaneous description of SC(m,n) and NSC(m,n) should give better constraints on the parameters in AMPT models.

6.2 Higher Order Harmonic Correlations

The higher order harmonic correlations (SC(4,3), SC(5,2) and SC(5,3)) are compared to several theoretical model calculations. The event-by-event EKRT+viscous hydrodynamic predictions with the different parameterizations for the temperature dependence of the shear viscosity to entropy density ratio $\eta/s(T)$ are shown in Fig. 5. While we discussed the comparison to these hydrodynamic model calculations with various temperature dependent η/s parameterizations, only two calculations with the parameters which describe the lower order harmonic correlations best are compared to the results of higher order harmonic correlations. As it can be seen in Fig. 1 from Ref. [30], for "param1" parameterization the phase transition from hadronic to QGP phase occurs at lowest temperature, already around 150 MeV. This parameterization is also characterized with moderate slope of $\eta/s(T)$ of decreasing (increasing) in hadronic (QGP) phase. The model calculations with the parameters for which the temperature of phase transition is larger than for "param1" can be ruled out already with the previous measurement [40]. As shown in Fig. 5, only the correlations between v_5 and v_2 are well described for all available centralities. On the other hand, for correlations between v_5 and v_3 the description fails in the transition towards more peripheral collisions, providing further independent constraints for the models. In the case of the correlation between v_4 and v_3, the same models underestimate the data significantly. Most notably, this measurement is so far the most dramatic example of a failure of constant η/s to describe the data.

The higher order harmonic correlations are compared to VISH2+1 calculations [41], shown in Fig. 6. All the models with large η/s ($\eta/s = 0.2$ for MC-KLN and MC-Glauber, and $\eta/s = 0.16$ for AMPT
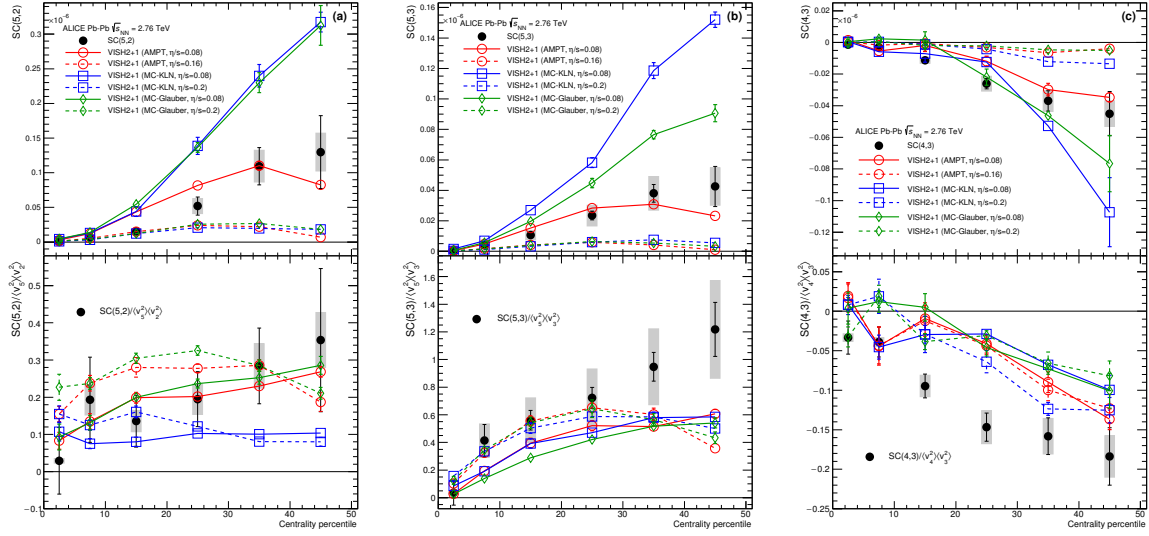
Fig. 6: Results of SC(5,2), SC(5,3) and SC(4,3) in Pb–Pb collisions at $\sqrt{s_{NN}} = 2.76$ TeV are compared to various VISH2+1 calculations [41]. Three initial conditions from AMPT, MC-KLN and MC-Glauber are drawn as different colors and markers. The η/s parameters are shown as different line styles, the small shear viscosity ($\eta/s = 0.08$) are shown as solid lines, and large shear viscosities ($\eta/s = 0.2$ for MC-KLN and MC-Glauber, 0.16 for AMPT) are drawn as dashed lines. Upper (lower) panels show SC(m,n) (NSC(m,n)).

initial conditions) regardless of the initial conditions fail to capture the centrality dependence of SC(5,2), SC(5,2) and SC(5,3), with larger disagreements than observed for the lower order harmonic correlations. Among the models with small η/s ($\eta/s = 0.08$), the one with the AMPT initial conditions describes the data much better than the ones with other initial conditions. A quite clear separation between different initial conditions is observed for these higher order harmonic correlations compared to the lower order harmonic correlations. NSC(5,2) and SC(5,3) are quite sensitive to both the initial conditions and the η/s parameterizations. Similar to the hydrodynamic calculations mentioned above [30], the sign of NSC(4,3) in these models is opposite to its sign in the data in 0-10% central collisions. NSC(4,3) shows sensitivity to both initial conditions and η/s parameterizations. The SC(4,3) results are clearly favored by smaller η/s values but NSC(4,3) cannot be described by these models quantitively.

The results from AMPT simulations are compared to the data in Fig. 7. The string melting AMPT model describes SC(5,3) and NSC(5,3) well. However, the same setting overestimates SC(5,2) and NSC(5,2). The default AMPT model can describe NSC(5,3) and NSC(5,2) fairly well as in the case of the lower harmonics seen in Fig. 4. In the case of SC(4,3), neither of the settings can describe the data but the default AMPT model comes the closest to the data. The string melting AMPT model fails to describe SC(4,3) and NSC(4,3). In summary, the default AMPT model describes well the normalized symmetric cumulants (NSC(m,n)) from lower to higher order harmonic correlations while the string melting AMPT model overestimates NSC(5,2) and predicts a very weak correlation in NSC(4,3).

As discussed in Sec. 5, a hierarchy NSC(5,3) > NSC(4,2) > NSC(5,2) holds for centrality ranges > 20% within the errors and NSC(5,2) is smaller than NSC(5,3) while SC(5,2) is larger that SC(5,3). Except for 0-10% centrality range, we found that the same hierarchy also holds in the hydrodynamic calculations and the AMPT models explored in this article. The observed reversal of the hierarchy SC(5,2) > SC(5,3), can be explained by the magnitudes of the individual flow harmonics ($v_2 > v_3$). The opposite trend is observed for the normalized SC (NSC(5,3) > NSC(5,2)). This can be attributed to the fact that flow fluctuations are stronger for v_3 than v_2 [80]. This was claimed in Ref. [41] and also seen in Ref. [81] based on a AMPT model. NSC(m,n) correlators increase with larger η/s in hydrodynamic calculations
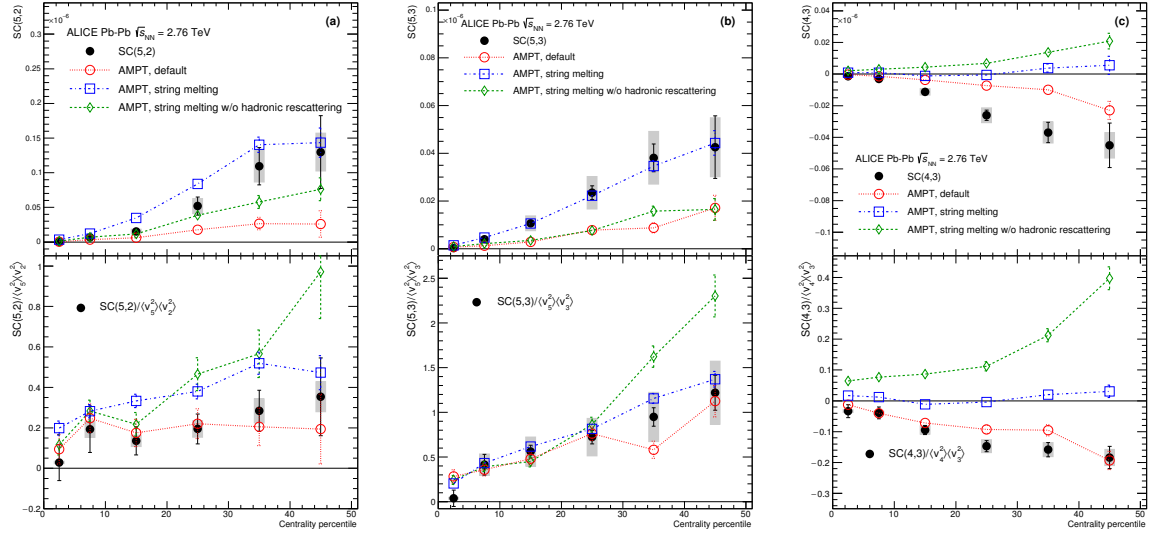
Fig. 7: Results of SC(5,2), SC(5,3) and SC(4,3) in Pb–Pb collisions at $\sqrt{s_{NN}} = 2.76$ TeV are compared to various AMPT models. Upper (lower) panels show SC(m,n) (NSC(m,n)).

in the 0-30% centrality range in the same way as the event plane correlations [82, 83]. In semi-peripheral collisions (>40%), the opposite trend is observed.

We list here the important findings from the model comparisons:

(i) All the VISH2+1 model calculations with large η/s fail to capture the centrality dependence of the correlations regardless of the initial conditions.

(ii) Among the VISH2+1 model calculations with small η/s ($\eta/s = 0.08$), the one with the AMPT initial conditions describes the data qualitatively but it cannot describe the data quantitively for most of the centrality ranges.

(iii) The NSC(3,2) observable is sensitive mainly to the initial conditions, while the other observables are sensitive to both the initial conditions and the temperature dependence of η/s.

(iv) The correlation strength between v_3 and v_2 and between v_4 and v_3 (NSC(3,2) and NSC(4,3)) is significantly underestimated in hydrodynamic model calculations.

(v) The sign of NSC(3,2) in 0-10% central collisions was found to be different in the data and the hydrodynamic model calculations while the default AMPT model can reproduce the sign.

(vi) The default AMPT model can describe the normalized symmetric cumulants (NSC(m,n)) quantitively for most centralities while the string melting AMPT model fails to describe them.

(vii) A hierarchy NSC(5,3) > NSC(4,2) > NSC(5,2) holds for centrality ranges > 20% within the errors. This hierarchy is reproduced well both by hydrodynamic and AMPT model calculations.

6.3 Transverse Momentum Dependence of Correlations between v_2, v_3 and v_4

It can be seen in Fig. 2 that for the NSC(3,2) observable no p_T dependence is seen in the centrality range <30%, and a moderate decreasing trend with increasing p_T is seen for the >30% centrality range. NSC(4,2) shows a moderate decreasing trend as p_T or the centrality increase. In order to see the trend more clearly, we show NSC(m,n) results as a function of minimum p_T cut in Fig. 8 and Fig. 9.
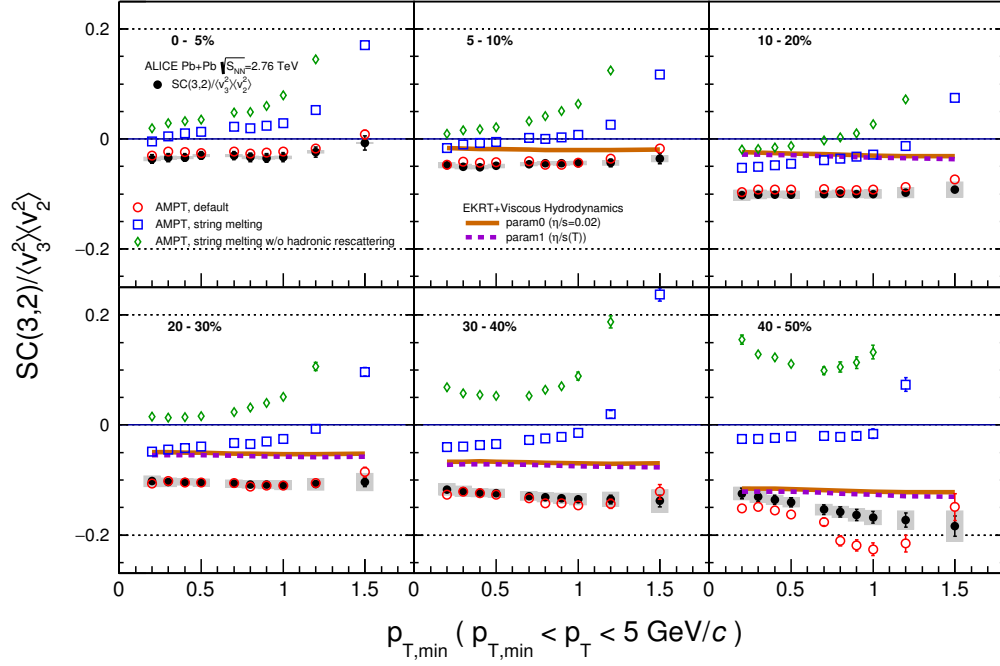
13

Fig. 8: NSC(3,2) as a function of the minimum p_T cuts in Pb–Pb collisions at $\sqrt{s_{NN}} = 2.76$ TeV are compared to various AMPT configurations and event-by-event EKRT+viscous hydrodynamic calculations [30].
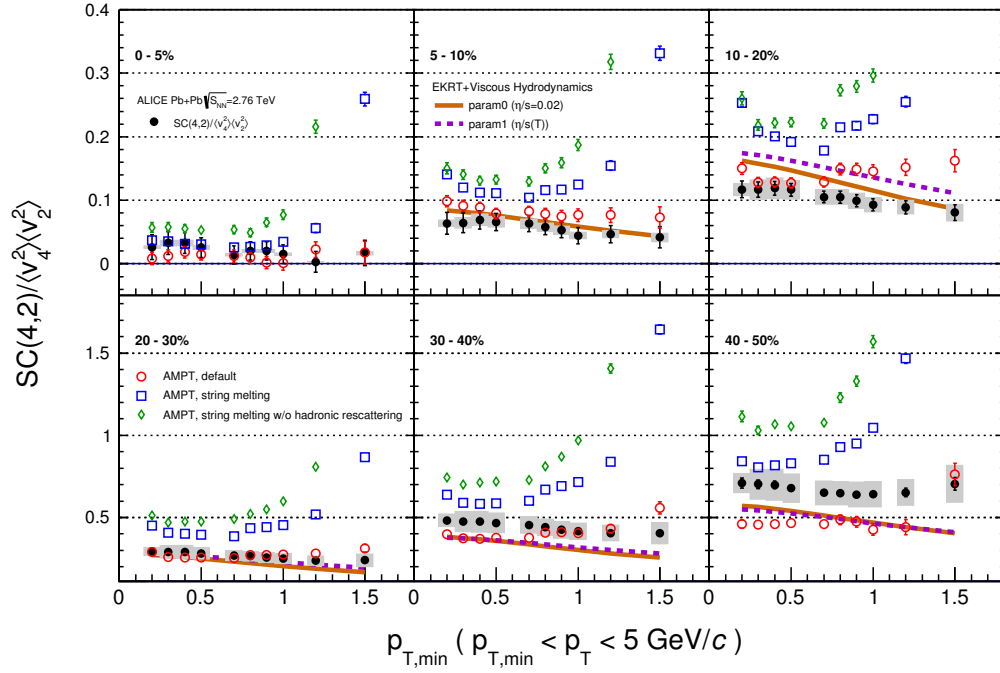

Fig. 9: NSC(4,2) as a function of the minimum p_T cuts in Pb–Pb collisions at $\sqrt{s_{NN}} = 2.76$ TeV are compared to various AMPT configurations and event-by-event EKRT+viscous hydrodynamic calculations [30].

NSC(3,2) and NSC(4,2) as a function of different minimum p_T cuts are compared to the AMPT simulations in Fig. 8 and Fig. 9, respectively. The observed p_T-dependence for NSC(3,2) and NSC(4,2) in mid-central collisions is also seen in AMPT simulations for higher minimum p_T cuts. With the exception of the default configuration, the other AMPT settings predict a very strong p_T dependence above 1 GeV/c and cannot describe the magnitude of the data for both NSC(3,2) and NSC(4,2) simultaneously. In the case of NSC(3,2), the default AMPT model describes the magnitude and p_T dependence well in all collision centralities except for $40 - 50\%$ where the model underestimates the data and shows a stronger p_T dependence than the data. As for NSC(4,2), the same model which describes NSC(3,2) can also reproduce the data well except for the $10 - 20\%$ and $40 - 50\%$ centralities where some deviations from the data are observed. When the string melting AMPT model is compared to the same model with the hadronic rescattering off, it is observed that the very strong p_T dependence as well as the correlation strength are weakened by the hadronic rescattering. This might imply that hadronic interactions are the source of this observed p_T dependence even though the relative contributions from the partonic and hadronic stages in the final state particle distributions should be studied further.

The event-by-event EKRT+viscous hydrodynamic calculations are compared to the data in Fig. 8. In case of NSC(3,2), the hydrodynamic calculations underestimate the data as discussed in Sec 6.1 and show very weak p_T dependence for all centralities. The p_T dependence of NSC(3,2) is well described by the model calculations in all collision centralities except for 40-50% where the data shows stronger p_T dependence than the models. The difference between the model calculations with the two parameterizations is very small. As for NSC(4,2), the model calculations overestimate the magnitude in the 5-20% centralities and underestimate in the centrality range >20%. However the p_T dependence is well described by the model calculations in all centralities. While the difference of the model calculations between two parameterizations in most centralities is rather small, the clear separation between two parameterizations are observed in 10-20% where both the magnitude and p_T dependence are different.

This observed moderate p_T dependence in mid-central collisions both for NSC(3,2) and NSC(4,2) might be an indication of possible viscous corrections to the equilibrium distribution at hadronic freeze-out as predicted in [21]. The comparisons to hydrodynamic models can further help to understand the viscous corrections to the momentum distributions at hadronic freeze-out [30, 36–39].

7 Summary

In this article, we report the centrality dependence of correlation between the higher order harmonics (v_3, v_4, v_5) and the lower order harmonics (v_2, v_3) as well as the transverse momentum dependence of the correlations between v_3 and v_2 and between v_4 and v_2. The results are obtained with Symmetric 2-harmonic 4-particle Cumulants (SC). It was demonstrated earlier in [40] that this method is insensitive to the nonflow effects and free from symmetry plane correlations. We have found that fluctuations of SC(3,2) and SC(4,3) are anti-correlated in all centralities while fluctuations of SC(4,2), SC(5,2) and SC(5,3) are correlated for all centralities. These measurements were compared to various hydrodynamic model calculations with different initial conditions as well as different parameterizations of the temperature dependence of η/s. It is found that the different order harmonic correlations have different sensitivities to the initial conditions and the system properties. Therefore they have discriminating power in separating the effects of η/s from the initial conditions on the final state particle anisotropies. The sign of SC(3,2) in 0-10% central collisions was found to be different between the data and hydrodynamic model calculations. In the most central collisions the anisotropies originate mainly from fluctuations, where the initial ellipsoidal geometry which dominates in mid-central collisions plays little role. This observation might help to understand the details of the fluctuations in the initial stage. The comparisons to VISH2+1 calculations show that all the models with large η/s, regardless of the initial conditions, fail to capture the centrality dependence of higher order correlations. Based on the tested model parameters, the data favors small η/s and the AMPT initial conditions. A quite clear separation of the correlation strength

for different initial conditions is observed for these higher order harmonic correlations compared to the lower order harmonic correlations. The default configuration of the AMPT model describes well the normalized symmetric cumulants (NSC(m,n)) for most centralities and for most combinations of harmonics which were considered. Together with the measurements of individual harmonics these results provide further constraints on the system properties and help discriminate between theoretical models. Finally, we have found that v_3 and v_2 as well as v_4 and v_2 correlations have moderate p_T dependence in mid-central collisions. This might be an indication of possible viscous corrections to the equilibrium distribution at hadronic freeze-out. The results presented in this article can be used to further optimize model parameters and put better constraints on the initial conditions and the transport properties of nuclear matter in ultra-relativistic heavy-ion collisions.

Acknowledgements

References

[1] **STAR** Collaboration, K. H. Ackermann *et al.*, "Elliptic flow in Au + Au collisions at (S(NN))**(1/2) = 130 GeV," *Phys. Rev. Lett.* **86** (2001) 402–407, `arXiv:nucl-ex/0009011 [nucl-ex]`.

[2] **ALICE** Collaboration, K. Aamodt *et al.*, "Elliptic flow of charged particles in Pb-Pb collisions at 2.76 TeV," *Phys. Rev. Lett.* **105** (2010) 252302, `arXiv:1011.3914 [nucl-ex]`.

[3] **ALICE** Collaboration, J. Adam *et al.*, "Anisotropic flow of charged particles in Pb-Pb collisions at $\sqrt{s_{NN}} = 5.02$ TeV," *Phys. Rev. Lett.* **116** no. 13, (2016) 132302, `arXiv:1602.01119 [nucl-ex]`.

[4] P. Romatschke and U. Romatschke, "Viscosity Information from Relativistic Nuclear Collisions: How Perfect is the Fluid Observed at RHIC?," *Phys. Rev. Lett.* **99** (2007) 172301, `arXiv:0706.1522 [nucl-th]`.

[5] C. Shen, U. Heinz, P. Huovinen, and H. Song, "Radial and elliptic flow in Pb+Pb collisions at the Large Hadron Collider from viscous hydrodynamic," *Phys. Rev.* **C84** (2011) 044903, `arXiv:1105.3226 [nucl-th]`.

[6] B. Schenke, S. Jeon, and C. Gale, "Elliptic and triangular flows in 3 + 1D viscous hydrodynamics with fluctuating initial conditions," *J. Phys.* **G38** (2011) 124169.

[7] P. Bozek and I. Wyskiel-Piekarska, "Particle spectra in Pb-Pb collisions at $\sqrt{S_NN} = 2.76 TeV$," *Phys. Rev.* **C85** (2012) 064915, `arXiv:1203.6513 [nucl-th]`.

[8] "Event-by-event anisotropic flow in heavy-ion collisions from combined Yang-Mills and viscous fluid dynamics," *Phys. Rev. Lett.* **110** no. 1, (2013) 012302, `arXiv:1209.6330 [nucl-th]`.

[9] T. Hirano, P. Huovinen, and Y. Nara, "Elliptic flow in Pb+Pb collisions at $\sqrt{s_{NN}} = 2.76$ TeV: hybrid model assessment of the first data," *Phys. Rev.* **C84** (2011) 011901, `arXiv:1012.3955 [nucl-th]`.

[10] P. Kovtun, D. T. Son, and A. O. Starinets, "Viscosity in strongly interacting quantum field theories from black hole physics," *Phys. Rev. Lett.* **94** (2005) 111601, `arXiv:hep-th/0405231 [hep-th]`.

[11] R. A. Lacey, N. N. Ajitanand, J. M. Alexander, P. Chung, W. G. Holzmann, M. Issah, A. Taranenko, P. Danielewicz, and H. Stoecker, "Has the QCD Critical Point been Signaled by Observations at RHIC?," *Phys. Rev. Lett.* **98** (2007) 092301, `arXiv:nucl-ex/0609025 [nucl-ex]`.

[12] P. Danielewicz and M. Gyulassy, "Dissipative phenomena in quark-gluon plasmas," *Phys. Rev. D* **31** (Jan, 1985) 53–62. http://link.aps.org/doi/10.1103/PhysRevD.31.53.

[13] L. P. Csernai, J. Kapusta, and L. D. McLerran, "On the Strongly-Interacting Low-Viscosity Matter Created in Relativistic Nuclear Collisions," *Phys. Rev. Lett.* **97** (2006) 152303, arXiv:nucl-th/0604032 [nucl-th].

[14] J.-Y. Ollitrault, "Anisotropy as a signature of transverse collective flow," *Phys. Rev.* **D46** (1992) 229–245.

[15] S. Voloshin and Y. Zhang, "Flow study in relativistic nuclear collisions by Fourier expansion of Azimuthal particle distributions," *Z. Phys.* **C70** (1996) 665–672, arXiv:hep-ph/9407282 [hep-ph].

[16] S. Floerchinger, U. A. Wiedemann, A. Beraudo, L. Del Zanna, G. Inghirami, and V. Rolando, "How (non-)linear is the hydrodynamics of heavy ion collisions?," *Phys. Lett.* **B735** (2014) 305–310, arXiv:1312.5482 [hep-ph].

[17] M. Miller and R. Snellings, "Eccentricity fluctuations and its possible effect on elliptic flow measurements," arXiv:nucl-ex/0312008 [nucl-ex].

[18] **PHOBOS** Collaboration, B. Alver *et al.*, "System size, energy, pseudorapidity, and centrality dependence of elliptic flow," *Phys. Rev. Lett.* **98** (2007) 242302, arXiv:nucl-ex/0610037 [nucl-ex].

[19] B. Alver and G. Roland, "Collision geometry fluctuations and triangular flow in heavy-ion collisions," *Phys. Rev.* **C81** (2010) 054905, arXiv:1003.0194 [nucl-th]. [Erratum: Phys. Rev.C82,039903(2010)].

[20] **ALICE** Collaboration, K. Aamodt *et al.*, "Higher harmonic anisotropic flow measurements of charged particles in Pb-Pb collisions at $\sqrt{s_{NN}}$=2.76 TeV," *Phys. Rev. Lett.* **107** (2011) 032301, arXiv:1105.3865 [nucl-ex].

[21] H. Niemi, G. S. Denicol, H. Holopainen, and P. Huovinen, "Event-by-event distributions of azimuthal asymmetries in ultrarelativistic heavy-ion collisions," *Phys. Rev.* **C87** no. 5, (2013) 054901, arXiv:1212.1008 [nucl-th].

[22] **ATLAS** Collaboration, G. Aad *et al.*, "Measurement of event-plane correlations in $\sqrt{s_{NN}} = 2.76$ TeV lead-lead collisions with the ATLAS detector," *Phys. Rev.* **C90** no. 2, (2014) 024905, arXiv:1403.0489 [hep-ex].

[23] B. H. Alver, C. Gombeaud, M. Luzum, and J.-Y. Ollitrault, "Triangular flow in hydrodynamics and transport theory," *Phys. Rev.* **C82** (2010) 034913, arXiv:1007.5469 [nucl-th].

[24] M. Luzum and J.-Y. Ollitrault, "Extracting the shear viscosity of the quark-gluon plasma from flow in ultra-central heavy-ion collisions," *Nucl. Phys.* **A904-905** (2013) 377c–380c, arXiv:1210.6010 [nucl-th].

[25] C. Shen, S. A. Bass, T. Hirano, P. Huovinen, Z. Qiu, H. Song, and U. Heinz, "The QGP shear viscosity: Elusive goal or just around the corner?," *J. Phys.* **G38** (2011) 124045, arXiv:1106.6350 [nucl-th].

[26] P. Bozek, "Flow and interferometry in 3+1 dimensional viscous hydrodynamics," *Phys. Rev.* **C85** (2012) 034901, arXiv:1110.6742 [nucl-th].

[27] J.-B. Rose, J.-F. Paquet, G. S. Denicol, M. Luzum, B. Schenke, S. Jeon, and C. Gale, "Extracting the bulk viscosity of the quark?gluon plasma," *Nucl. Phys.* **A931** (2014) 926–930, `arXiv:1408.0024 [nucl-th]`.

[28] S. Ryu, J. F. Paquet, C. Shen, G. S. Denicol, B. Schenke, S. Jeon, and C. Gale, "Importance of the Bulk Viscosity of QCD in Ultrarelativistic Heavy-Ion Collisions," *Phys. Rev. Lett.* **115** no. 13, (2015) 132301, `arXiv:1502.01675 [nucl-th]`.

[29] D. Teaney and L. Yan, "Triangularity and Dipole Asymmetry in Heavy Ion Collisions," *Phys. Rev.* **C83** (2011) 064904, `arXiv:1010.1876 [nucl-th]`.

[30] H. Niemi, K. J. Eskola, and R. Paatelainen, "Event-by-event fluctuations in a perturbative QCD + saturation + hydrodynamics model: Determining QCD matter shear viscosity in ultrarelativistic heavy-ion collisions," *Phys. Rev.* **C93** no. 2, (2016) 024907, `arXiv:1505.02677 [hep-ph]`.

[31] Z. Qiu and U. W. Heinz, "Event-by-event shape and flow fluctuations of relativistic heavy-ion collision fireballs," *Phys. Rev.* **C84** (2011) 024911, `arXiv:1104.0650 [nucl-th]`.

[32] S. S. Gubser and A. Yarom, "Conformal hydrodynamics in Minkowski and de Sitter spacetimes," *Nucl. Phys.* **B846** (2011) 469–511, `arXiv:1012.1314 [hep-th]`.

[33] Y. Hatta, J. Noronha, G. Torrieri, and B.-W. Xiao, "Flow harmonics within an analytically solvable viscous hydrodynamic model," *Phys. Rev.* **D90** no. 7, (2014) 074026, `arXiv:1407.5952 [hep-ph]`.

[34] L. V. Bravina, B. H. Brusheim Johansson, G. K. Eyyubova, V. L. Korotkikh, I. P. Lokhtin, L. V. Malinina, S. V. Petrushanko, A. M. Snigirev, and E. E. Zabrodin, "Higher harmonics of azimuthal anisotropy in relativistic heavy ion collisions in HYDJET++ model," *Eur. Phys. J.* **C74** no. 3, (2014) 2807, `arXiv:1311.7054 [nucl-th]`.

[35] L. V. Bravina, B. H. Brusheim Johansson, G. K. Eyyubova, V. L. Korotkikh, I. P. Lokhtin, L. V. Malinina, S. V. Petrushanko, A. M. Snigirev, and E. E. Zabrodin, "Hexagonal flow v6 as a superposition of elliptic v2 and triangular v3 flows," *Phys. Rev.* **C89** no. 2, (2014) 024909, `arXiv:1311.0747 [hep-ph]`.

[36] D. Teaney and L. Yan, "Non linearities in the harmonic spectrum of heavy ion collisions with ideal and viscous hydrodynamics," *Phys. Rev.* **C86** (2012) 044908, `arXiv:1206.1905 [nucl-th]`.

[37] M. Luzum and J.-Y. Ollitrault, "Constraining the viscous freeze-out distribution function with data obtained at the BNL Relativistic Heavy Ion Collider (RHIC)," *Phys. Rev.* **C82** (2010) 014906, `arXiv:1004.2023 [nucl-th]`.

[38] K. Dusling, G. D. Moore, and D. Teaney, "Radiative energy loss and v(2) spectra for viscous hydrodynamics," *Phys. Rev.* **C81** (2010) 034907, `arXiv:0909.0754 [nucl-th]`.

[39] D. Molnar and Z. Wolff, "Self-consistent conversion of a viscous fluid to particles," `arXiv:1404.7850 [nucl-th]`.

[40] **ALICE** Collaboration, J. Adam *et al.*, "Correlated event-by-event fluctuations of flow harmonics in Pb-Pb collisions at $\sqrt{s_{\mathrm{NN}}} = 2.76$ TeV," *Phys. Rev. Lett.* **117** (2016) 182301, `arXiv:1604.07663 [nucl-ex]`.

[41] X. Zhu, Y. Zhou, H. Xu, and H. Song, "Correlations of flow harmonics in 2.76A TeV Pb–Pb collisions," `arXiv:1608.05305 [nucl-th]`.

[42] H. Niemi, G. S. Denicol, P. Huovinen, E. Molnar, and D. H. Rischke, "Influence of the shear viscosity of the quark-gluon plasma on elliptic flow in ultrarelativistic heavy-ion collisions," *Phys. Rev. Lett.* **106** (2011) 212302, arXiv:1101.2442 [nucl-th].

[43] A. Bilandzic, C. H. Christensen, K. Gulbrandsen, A. Hansen, and Y. Zhou, "Generic framework for anisotropic flow analyses with multiparticle azimuthal correlations," *Phys. Rev.* **C89** no. 6, (2014) 064904, arXiv:1312.3572 [nucl-ex].

[44] G. Giacalone, L. Yan, J. Noronha-Hostler, and J.-Y. Ollitrault, "Symmetric cumulants and event-plane correlations in Pb + Pb collisions," *Phys. Rev.* **C94** no. 1, (2016) 014906, arXiv:1605.08303 [nucl-th].

[45] **ALICE** Collaboration, K. Aamodt *et al.*, "The ALICE experiment at the CERN LHC," *JINST* **3** (2008) S08002.

[46] **ALICE** Collaboration, P. Cortese *et al.*, "ALICE: Physics performance report, volume I," *J. Phys.* **G30** (2004) 1517–1763.

[47] **ALICE** Collaboration, P. Cortese *et al.*, "ALICE: Physics performance report, volume II," *J. Phys.* **G32** (2006) 1295–2040.

[48] **ALICE** Collaboration, K. Aamodt *et al.*, "Centrality dependence of the charged-particle multiplicity density at mid-rapidity in Pb-Pb collisions at $\sqrt{s_{NN}} = 2.76$ TeV," *Phys. Rev. Lett.* **106** (2011) 032301, arXiv:1012.1657 [nucl-ex].

[49] X.-N. Wang and M. Gyulassy, "HIJING: A Monte Carlo model for multiple jet production in p p, p A and A A collisions," *Phys. Rev.* **D44** (1991) 3501–3516.

[50] "GEANT Detector Description and Simulation Tool,".

[51] **ALICE** Collaboration, E. Abbas *et al.*, "Performance of the ALICE VZERO system," *JINST* **8** (2013) P10016, arXiv:1306.3130 [nucl-ex].

[52] **ALICE** Collaboration, G. Dellacasa *et al.*, "ALICE technical design report of the inner tracking system (ITS),".

[53] S. A. Voloshin, A. M. Poskanzer, and R. Snellings, "Collective phenomena in non-central nuclear collisions," arXiv:0809.2949 [nucl-ex].

[54] **ALICE** Collaboration, B. Abelev *et al.*, "Anisotropic flow of charged hadrons, pions and (anti-)protons measured at high transverse momentum in Pb-Pb collisions at $\sqrt{s_{NN}}$=2.76 TeV," *Phys. Lett.* **B719** (2013) 18–28, arXiv:1205.5761 [nucl-ex].

[55] R. Paatelainen, K. J. Eskola, H. Holopainen, and K. Tuominen, "Multiplicities and p_T spectra in ultrarelativistic heavy ion collisions from a next-to-leading order improved perturbative QCD + saturation + hydrodynamics model," *Phys. Rev.* **C87** no. 4, (2013) 044904, arXiv:1211.0461 [hep-ph].

[56] R. Paatelainen, K. J. Eskola, H. Niemi, and K. Tuominen, "Fluid dynamics with saturated minijet initial conditions in ultrarelativistic heavy-ion collisions," *Phys. Lett.* **B731** (2014) 126–130, arXiv:1310.3105 [hep-ph].

[57] C. Shen, U. Heinz, P. Huovinen, and H. Song, "Systematic parameter study of hadron spectra and elliptic flow from viscous hydrodynamic simulations of Au+Au collisions at $\sqrt{s_{NN}} = 200$ GeV," *Phys. Rev.* **C82** (2010) 054904, arXiv:1010.1856 [nucl-th].

[58] C. Shen, Z. Qiu, H. Song, J. Bernhard, S. Bass, and U. Heinz, "The iEBE-VISHNU code package for relativistic heavy-ion collisions," *Comput. Phys. Commun.* **199** (2016) 61–85, arXiv:1409.8164 [nucl-th].

[59] Z. Qiu, C. Shen, and U. Heinz, "Hydrodynamic elliptic and triangular flow in Pb-Pb collisions at $\sqrt{s} = 2.76$ATeV," *Phys. Lett.* **B707** (2012) 151–155, arXiv:1110.3033 [nucl-th].

[60] R. S. Bhalerao, A. Jaiswal, and S. Pal, "Collective flow in event-by-event partonic transport plus hydrodynamics hybrid approach," *Phys. Rev.* **C92** no. 1, (2015) 014903, arXiv:1503.03862 [nucl-th].

[61] P. F. Kolb, J. Sollfrank, and U. W. Heinz, "Anisotropic transverse flow and the quark hadron phase transition," *Phys. Rev.* **C62** (2000) 054909, arXiv:hep-ph/0006129 [hep-ph].

[62] D. Kharzeev and M. Nardi, "Hadron production in nuclear collisions at RHIC and high density QCD," *Phys. Lett.* **B507** (2001) 121–128, arXiv:nucl-th/0012025 [nucl-th].

[63] M. L. Miller, K. Reygers, S. J. Sanders, and P. Steinberg, "Glauber modeling in high energy nuclear collisions," *Ann. Rev. Nucl. Part. Sci.* **57** (2007) 205–243, arXiv:nucl-ex/0701025 [nucl-ex].

[64] H. J. Drescher and Y. Nara, "Effects of fluctuations on the initial eccentricity from the Color Glass Condensate in heavy ion collisions," *Phys. Rev.* **C75** (2007) 034905, arXiv:nucl-th/0611017 [nucl-th].

[65] T. Hirano and Y. Nara, "Eccentricity fluctuation effects on elliptic flow in relativistic heavy ion collisions," *Phys. Rev.* **C79** (2009) 064904, arXiv:0904.4080 [nucl-th].

[66] L. Pang, Q. Wang, and X.-N. Wang, "Effects of initial flow velocity fluctuation in event-by-event (3+1)D hydrodynamics," *Phys. Rev.* **C86** (2012) 024911, arXiv:1205.5019 [nucl-th].

[67] H.-j. Xu, Z. Li, and H. Song, "High-order flow harmonics of identified hadrons in 2.76A TeV Pb + Pb collisions," *Phys. Rev.* **C93** no. 6, (2016) 064905, arXiv:1602.02029 [nucl-th].

[68] B. Zhang, C. M. Ko, B.-A. Li, and Z.-w. Lin, "A multiphase transport model for nuclear collisions at RHIC," *Phys. Rev.* **C61** (2000) 067901, arXiv:nucl-th/9907017 [nucl-th].

[69] Z.-w. Lin, S. Pal, C. M. Ko, B.-A. Li, and B. Zhang, "Charged particle rapidity distributions at relativistic energies," *Phys. Rev.* **C64** (2001) 011902, arXiv:nucl-th/0011059 [nucl-th].

[70] Z.-W. Lin, C. M. Ko, B.-A. Li, B. Zhang, and S. Pal, "A Multi-phase transport model for relativistic heavy ion collisions," *Phys. Rev.* **C72** (2005) 064901, arXiv:nucl-th/0411110 [nucl-th].

[71] A. Kurkela and Y. Zhu, "Isotropization and hydrodynamization in weakly coupled heavy-ion collisions," *Phys. Rev. Lett.* **115** no. 18, (2015) 182301, arXiv:1506.06647 [hep-ph].

[72] M. Gyulassy and X.-N. Wang, "HIJING 1.0: A Monte Carlo program for parton and particle production in high-energy hadronic and nuclear collisions," *Comput. Phys. Commun.* **83** (1994) 307, arXiv:nucl-th/9502021 [nucl-th].

[73] B. Andersson, G. Gustafson, and B. Nilsson-Almqvist, "A Model for Low p(t) Hadronic Reactions, with Generalizations to Hadron - Nucleus and Nucleus-Nucleus Collisions," *Nucl. Phys.* **B281** (1987) 289–309.

[74] B. Nilsson-Almqvist and E. Stenlund, "Interactions Between Hadrons and Nuclei: The Lund Monte Carlo, Fritiof Version 1.6," *Comput. Phys. Commun.* **43** (1987) 387.

[75] B. Zhang, "ZPC 1.0.1: A Parton cascade for ultrarelativistic heavy ion collisions," *Comput. Phys. Commun.* **109** (1998) 193–206, arXiv:nucl-th/9709009 [nucl-th].

[76] B. Li, A. T. Sustich, B. Zhang, and C. M. Ko, "Studies of superdense hadronic matter in a relativistic transport model," *Int. J. Mod. Phys.* **E10** (2001) 267–352.

[77] Z.-w. Lin and C. M. Ko, "Partonic effects on the elliptic flow at RHIC," *Phys. Rev.* **C65** (2002) 034904, arXiv:nucl-th/0108039 [nucl-th].

[78] Z.-W. Lin, "Evolution of transverse flow and effective temperatures in the parton phase from a multi-phase transport model," *Phys. Rev.* **C90** no. 1, (2014) 014904, arXiv:1403.6321 [nucl-th].

[79] **ALICE** Collaboration, J. Adam *et al.*, "Higher harmonic flow coefficients of identified hadrons in Pb-Pb collisions at $\sqrt{s_{NN}}$ = 2.76 TeV," *JHEP* **09** (2016) 164, arXiv:1606.06057 [nucl-ex].

[80] **ATLAS** Collaboration, G. Aad *et al.*, "Measurement of the distributions of event-by-event flow harmonics in lead-lead collisions at = 2.76 TeV with the ATLAS detector at the LHC," *JHEP* **11** (2013) 183, arXiv:1305.2942 [hep-ex].

[81] R. S. Bhalerao, J.-Y. Ollitrault, and S. Pal, "Characterizing flow fluctuations with moments," *Phys. Lett.* **B742** (2015) 94–98, arXiv:1411.5160 [nucl-th].

[82] R. S. Bhalerao, J.-Y. Ollitrault, and S. Pal, "Event-plane correlators," *Phys. Rev.* **C88** (2013) 024909, arXiv:1307.0980 [nucl-th].

[83] D. Teaney and L. Yan, "Event-plane correlations and hydrodynamic simulations of heavy ion collisions," *Phys. Rev.* **C90** no. 2, (2014) 024902, arXiv:1312.3689 [nucl-th].

A The ALICE Collaboration